

# The MOORA method integrated finite element analysis of thin-wall tube structures for energy absorption in the front bumper

**Mustafa Yurdakul**

Gazi University

**İbrahim Ülke**

Gazi University

**Bekir Batuhan Sağol**

Gazi University

**Yusuf Tansel İç** (✉ [yustanic@baskent.edu.tr](mailto:yustanic@baskent.edu.tr))

Baskent University

---

## Research Article

**Keywords:** Tube structures, Energy absorption, Oblique compression, direct compression, finite element analysis, MOORA method

**Posted Date:** November 1st, 2022

**DOI:** <https://doi.org/10.21203/rs.3.rs-2210096/v1>

**License:**  This work is licensed under a Creative Commons Attribution 4.0 International License.

[Read Full License](#)

---

# The MOORA method integrated finite element analysis of thin-wall tube structures for energy absorption in the front bumper

Mustafa Yurdakul<sup>a</sup>, İbrahim Ülke<sup>a</sup>, Bekir Batuhan Sağol<sup>a</sup>, Yusuf Tansel İç<sup>b1</sup>

<sup>a</sup> Department of Mechanical Engineering, Gazi University, 06570, Maltepe, Ankara, Turkey.

<sup>b</sup> Department of Industrial Engineering, Baskent University, 06790, Maltepe, Ankara, Turkey.

[yurdakul@gazi.edu.tr](mailto:yurdakul@gazi.edu.tr); [ibrahimulke@gazi.edu.tr](mailto:ibrahimulke@gazi.edu.tr); [bekirsagol160@gmail.com](mailto:bekirsagol160@gmail.com); [yustanic@baskent.edu.tr](mailto:yustanic@baskent.edu.tr)

## Abstract

The developing world economy and the increasing income level cause the number of vehicles on the highways to increase rapidly. The increasing number of vehicles makes the highways more unsafe and increases the probability of accidents. This study is concerned with the dynamic analysis of axial and oblique compression in thin-walled tubes. Tubes under the effect of axial and oblique compression were compared with different cross-section profiles in terms of performance. Collision energy absorbed, crushing force efficiency, peak force, and velocity graphs are discussed in these performance parameters. The collision of the plates is discussed considering the speed and mass parameters that have entered the tubes using different cross-sections. Also, we developed a MOORA model integrated finite element analysis to rank the different alternative structures for different simulation cases. The MOORA model's ranking results presented the most suitable cross-section profiles that will provide the most appropriate damping result.

**Keywords:** Tube structures, Energy absorption, Oblique compression, direct compression, finite element analysis, MOORA method.

---

<sup>1</sup> Corresponding Author. [Tel:+90 312 2466664](tel:+903122466664). E-mail: [yustanic@baskent.edu.tr](mailto:yustanic@baskent.edu.tr)

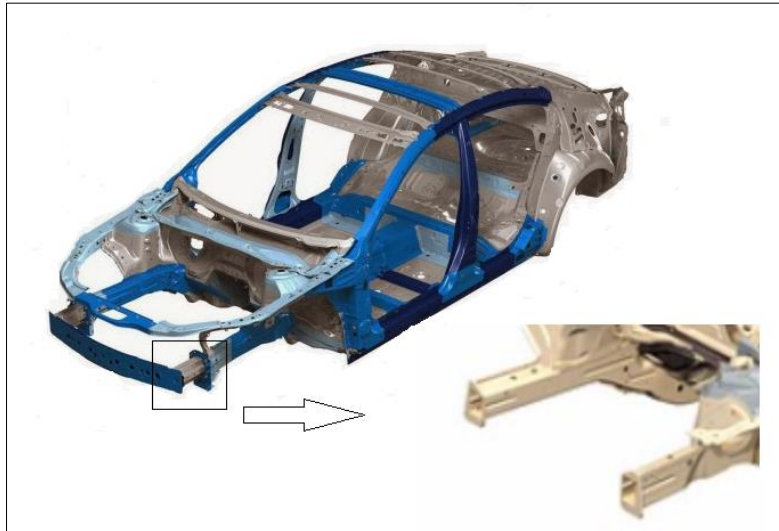
## **1. Introduction**

The energy that emerges in the event of a possible accident is first transferred to the bumpers [1-3]. In a possible crash, bumpers deform to reduce the kinetic energy transmitted to the vehicle by absorbing it. Thus, we minimized the damage to the passengers in the car. For this reason, bumpers are critical for the protection of human life [4]. Square or circular cross-sections are the most common thin wall structures for bumpers [5]. The deformation of the front of the vehicle may cause an undesirable situation in terms of safety considering moving toward the passenger compartment in case of a frontal collision of vehicles. In such accidents, the effects of inertia are reduced by damping the kinetic energy of the vehicle. So, the unsafe possibility of the persons can diminish in the vehicle.

Shock absorbers (Figure 1) are used behind the front bumper to cause less damage to the passenger compartment in case of a frontal collision of vehicles [6, 7]. Shock absorbers absorb the kinetic energy of the vehicle at a certain rate by undergoing plastic deformation. If shock-absorbing profiles are designed considering their damping properties, these profiles can be folded like an accordion to reduce the negative effects of the collision. In the event of a frontal collision, a certain part of the energy is absorbed by the shock absorbers after the bumper receives the first impact. Absorption of energy occurs by folding the front shock absorbers in an accordion shape and undergoing plastic deformation. In the first moments of the crash, the bumper deforms by absorbing a certain amount of energy. Then the shock absorbers begin to deform, and the reaction force in the axial direction reaches its highest value. Hence, the reaction forces begin to oscillate around an average value. Meanwhile, the structure becomes shorter by folding together with local sprains.

In this study, profiles of shock absorbers using absorb the kinetic energy of the impact in case of a crash and reduce the progress of deformation to the driver and passenger area were created and analyzed. We modeled shock absorbers and created the finite element models for

dynamic impact tests using the Abaqus (Simulia) software. Also, we developed a MOORA model to rank the alternative shock absorbers for different simulation scenarios' results and proposed the most suitable shock absorbers for different scenarios.



**Figure 1.** Thin shock absorber structure

In section 2, we present the literature review. In section 3, the methodology is presented. In section 4, design issues are discussed, and different structures are developed. In section 5, the results are presented. In section 6, findings and discussions are presented. Finally, in Section 7, the conclusion is presented.

## **2. Literature Review**

Researchers presented many studies on the finite element analysis (FEA) of tube structures for energy absorption in the front bumper. Li et al. [1] studied the improvement of the vehicle's frontal crashworthiness through front rail design. They conducted FEA analysis and verified it by experimental design. Basith et al. [8] studied the impact analysis of a bumper for three different materials. Khedkar et al. [9] analyzed thin-wall bumper beams using three different geometries. They discussed the energy absorption capacity of the bumpers. However, Askar and Ermis [10] investigated the size optimization of thin wall bumpers. They analyzed 25

different crash scenarios and found an optimal thickness for thin-wall structures. Lei et al. [11] investigated the optimization of front bumpers for the protection of pedestrians. They developed an algorithm under multiple impact situations. Sun et al. [12] developed a new approach for optimal buffer design under multiple low-velocity impact loads. They showed that the design with multiple load cases presents a general optimum. Wang et al. [13] performed a Six Sigma sturdiness optimization process based on the developed model for thin-wall structures. Kim et al. [14] investigated the elastic metal bumper's behavior under the hyper-speed impact. Their study showed that the shape effect can be reduced by using thinner and denser metal materials instead of aluminum. Wang et al. [15] conducted both the structural design and multi-purpose optimization of a thin-wall bumper system. The results showed that the crashworthiness issues of the vehicles can be significantly improved using the ESA algorithm. In addition to these studies, researchers have focused on bumper materials in many studies [16-22]. Goyal et al. [23] investigated the crashworthiness of star section bumpers. In their studies, they used structural topology optimization on various foam-filled tubes. Keni et al. [24] investigated the effects of wall thickness on crashworthiness by using the finite element method. They selected 2mm and 4mm wall thicknesses for comparative analysis. Zhang [25], Wang [26], Natarajan, Joshi, and Tyagi [27] focused on the crashworthiness improvement of bumpers during low impact speeds. They found that section profile and material type are the most efficient parameters on crashworthiness. Various studies have achieved developing the kinetic energy absorption capacity of thin-wall structures and investigated their optimal design. However, in most of the studies, researchers used one-way loading. But vehicle bumpers were subjected to different types of loads. Although the comprehensive analysis was used in the studies, the different section profiles weren't considered in detail. We discussed the crashworthiness and energy absorption capacity of 4 different types of thin-wall tube structures for direct and oblique impact.

### 3. Methodology

#### 3.1. Finite Element Modeling

Analysis methods with finite element methods are used extensively in product development stages in the automotive industry. Dynamic collision analysis is one of these methods, and this type of analysis is performed in much software. This software uses implicit (closed) and explicit (open) time integration methods for impact analysis [28, 29]. If there are varying sizes in very minimal time intervals as in multiplication problems, the open time integration method is used for such analyzes. Integration of the equation of motion in the time domain is calculated by the central differences method. In the first step, the following equation of motion is solved:

$$M \times a = P - I \quad (1)$$

Where, P: external forces, I: element internal forces, M: mass matrix, a: acceleration.

Acceleration value at time t is calculated as follows:

$$a_{(t)} = (M)^{-1} \times (P-I)_{(t)} \quad (2)$$

With the central difference methods, the acceleration is integrated in the time domain and the velocity is calculated as follows:

$$a'_{(t+Dt/2)} = a'_{(t-Dt/2)} + \frac{Dt_{(t+Dt)} + Dt_{(t)}}{2} \quad (3)$$

The displacement values at the node points are;

$$a_{(t+Dt)} = a_{(t)} + Dt_{(t+Dt)} a'_{(t+\frac{Dt}{2})} \quad (4)$$

In the first step, acceleration is found by achieving an equilibrium equation. By knowing the acceleration, velocity and displacements can be calculated for the next steps. In terms of the accuracy and stability of the calculated values, the time increment value ( $\Delta t$ ) should be chosen quite small. Thus, for small-time increments, the acceleration value can be assumed to be constant [30]. Additionally, taking the time increment value is too small increases the solution time. However, the equation set solution is not performed for the solution process in each

step. Therefore, the solution for each step is short. The choice of the time increment value is important for the stability of the solution. The following equation is used for analysis.

$$\Delta t_{\text{stable}} = L/c \quad (5)$$

The  $\Delta t$  value chosen must be less than or equal to the  $\Delta t_{\text{stable}}$  value. Here  $c$  is a characteristic feature of the sound velocity and the  $L$  is the smallest element length in finite element model;

$$c = \sqrt{\frac{E}{\rho}} \quad (6)$$

It is calculated by the equation. ( $E$ : modulus of elasticity,  $\rho$ : density)

After the calculation of the displacement values, the strain and stress values are found. Then, the element internal forces (1) are found, the time increment  $t + \Delta t$  are done and the next step is solved.

### 3.2. The MOORA method

The Multi-Objective Optimization based on Ratio Analysis (MOORA) method is a multi-criteria decision-making method used to select or rank independent alternatives. This method allows the performance of different alternatives for various purposes to be compared with numerical values. There is no MOORA study on thin-wall structure performance evaluation and its applications in the literature. The most important advantage of the MOORA method compared to other MCDM methods is that it has fewer application steps, and it is convenient to add and remove new alternatives and criteria easily (Table 1). Although there are many multi-criteria decision-making methods in the literature, the advantages of the MOORA method over other methods are given in Table 1 comparatively.

Table 1. Comparison of MOORA method with similar methods [31]

Methods	Modeling and solving time	Modeling simplicity	Computation complexity	Additional modeling requirements
MOORA	Very low	Very simple	Very low	No
TOPSIS	Medium	Normal	Medium	No
VIKOR	High	Normal	High	Yes
ELECTRE	Very High	Normal	Very High	Yes
AHP	Very High	Very critical	Very High	Yes
PROMETHEE	Very High	Critical	Very High	Yes

As can be seen in Table 1, the MOORA method is easy to apply, but it is a suitable method for practical practitioners, especially in the industry, where successful ranking results can be obtained competitively with other methods. Due to this feature, the MOORA method was used in our study.

In the first step of the MOORA method, the objectives (criteria) of the decision problem and the performance values of different alternatives according to these objectives are determined numerically. According to the determined values, an  $m \times n$  dimensional decision matrix shown in Eq.(7) is created [32,33]. The matrix columns show the selection criteria, and the matrix rows show the alternatives.

$$X = \begin{bmatrix} X_{11} & X_{12} & \dots & X_{1n} \\ X_{21} & X_{22} & \dots & X_{2n} \\ \cdot & \cdot & \dots & \cdot \\ \cdot & \cdot & \dots & \cdot \\ \cdot & \cdot & \dots & \cdot \\ X_{m1} & X_{m2} & \dots & X_{mn} \end{bmatrix} \quad (7)$$

After the decision matrix is created, the matrix is normalized for the application of the MOORA method by using Eq.(8) with  $i=1,2,\dots,m$  number of different alternatives,  $j=1,2,\dots,n$  criteria.

$$x_{ij}^* = \frac{x_{ij}}{\sqrt{\sum_{j=1}^m x_{ij}^2}}, \quad x_{ij}^* \in [0,1] \quad (8)$$



After the normalization process, the largest and smallest values of the criteria are determined. Then, reference points for all alternatives and weights of all criteria are calculated. The sum of the weight values of the criteria ( $w_j$ ) is equal to 1, as shown in Eq.(9).

$$\sum_{j=1}^n w_j = 1 \quad (9)$$

The ranking scores of the alternatives are calculated with the formula in Eq.(10) using the weight values of each criterion [32,33].

$$y_i^* = \sum_{j=1}^n w_j x_{ij}^* \quad (10)$$

where,  $y_i^*$  indicates the MOORA ranking score.




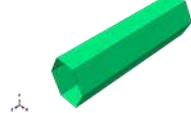
#### 4. Design

Four different thin tube section profiles in the form of a circle, square, rectangle, and hexagon were investigated in this study. The tubular building material is modeled as A36 material, which is a mild steel type (Table 2). When designing these structures, the circumference, length, and thickness of the sections were kept constant. The length was selected as 350 mm, and thickness was selected as 2 mm. For the cross-sectional circumference, all tube profiles were chosen to be 300 mm. These values were selected for the average circumference of most sedans available in the global market [34]. When the previous studies were examined, it was determined that the highest load increase occurred at 30° without a large decrease in the average force. The first impact velocities were set at 15.6 m/s with impact masses of 275 kg, 500 kg, 700 kg, and 1000 kg. Profiles and dimensions of thin wall tubes are given in Table 3.

**Table 2.** Some values for A36 mild steel material

Parameter	Value
A	146.7 MPa
B	896.9 MPa
N	0.320
C	0.033
M	0.323
T <sub>m</sub>	1773 K
C <sub>p</sub>	486 J/kg-°K
ε <sub>0</sub>	1.0 s <sup>-1</sup>
ρ	7850 kg/m <sup>3</sup>

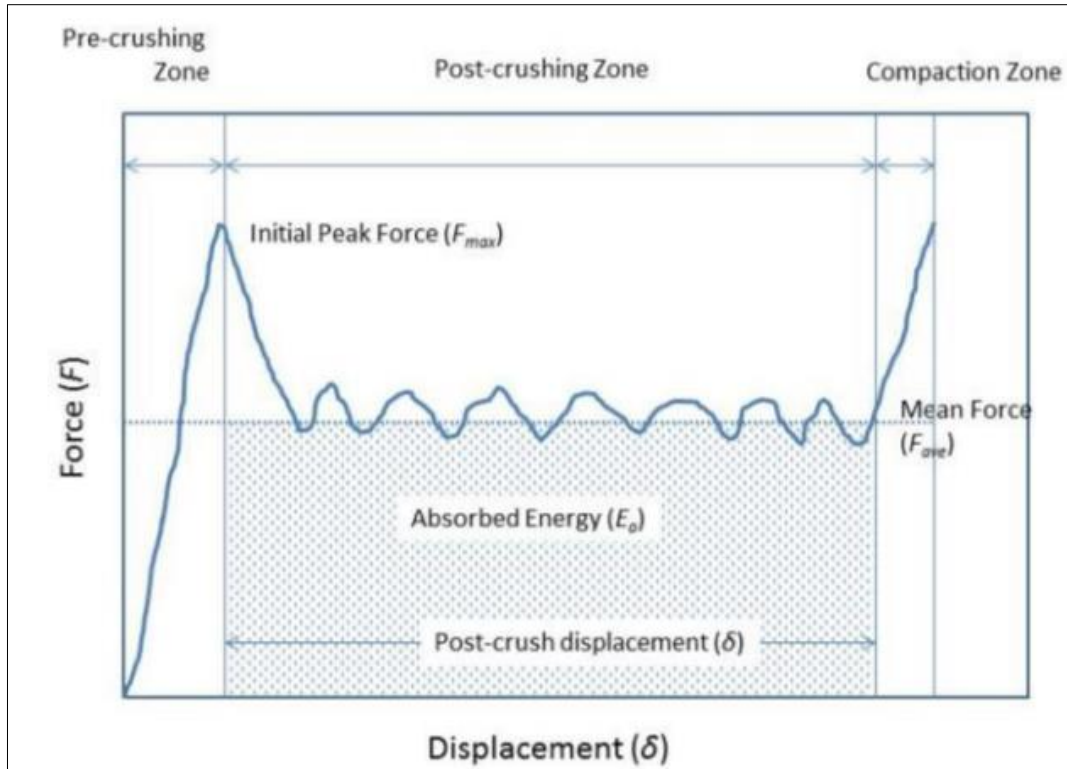
**Table 3.** Profile and dimensions of thin wall tubes

Profile	Perimeter (mm)	Length (mm)	Mass (kg)	Section Dimension (mm)	Thickness (mm)	Profile
Circular	300	350	1.7	D=95.5	2	
Rectangle	300	350	1.7	90 x 60	2	
Square	300	350	1.7	75 x 75	2	
Hexagonal	300	350	1.7	50 each side	2	

The following parameters were obtained under the crash response:

1. Peak Force, (**F<sub>MAX</sub>**)
2. Energy Absorption, (**E<sub>s</sub>**)
3. Crush force efficiency, (**CFE**)

In summary, the most useful energy absorber should reach the peak load rapidly and then values of the average load close to this peak load (Figure 2). The absorber should maintain this over the entire length of the component.



**Figure 2.** Typical force-displacement diagram

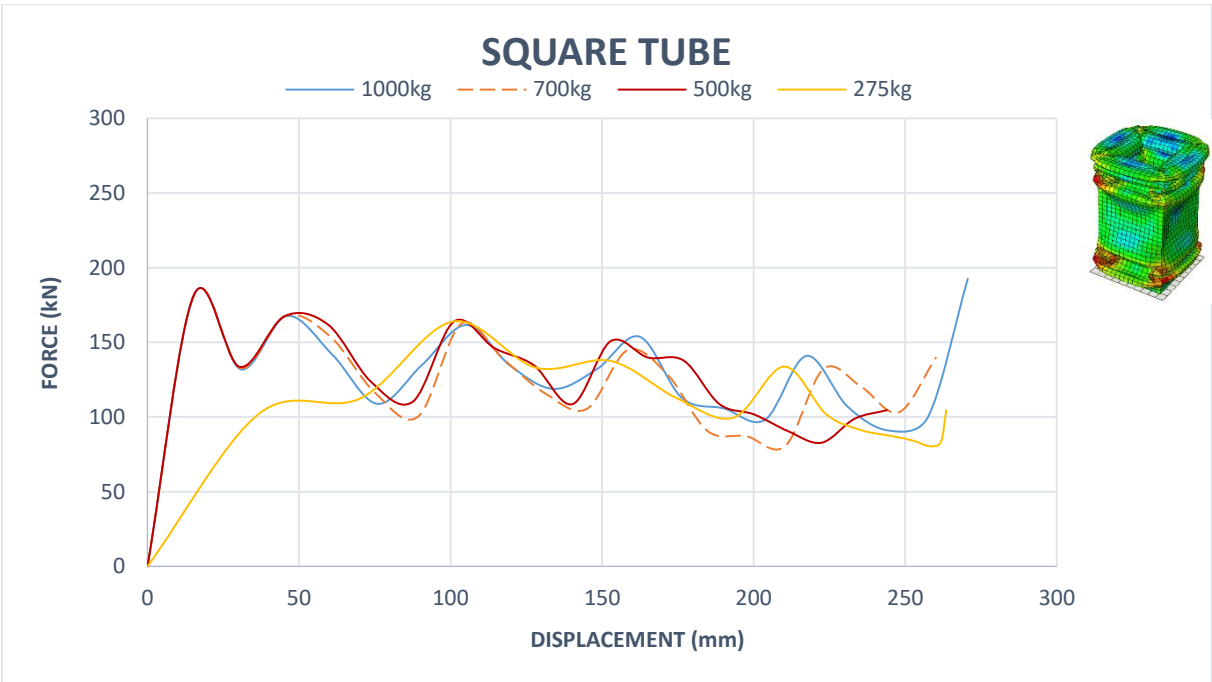
Finite element models of thin-wall structures were developed by using the ABAQUS Explicit in this study. The model in this study mainly consists of the thin-wall structure under two types of loading. Element sizes were selected as 5 mm for the thin wall tubes. A general contact algorithm was used for simulations. The Coulomb coefficient of friction value for all contact surfaces was selected as 0.2.

The striker was selected as a rigid body, translation, and rotational degrees of freedom were fixed at the given values except for only one allowable translational displacement. The impact velocity of the impactor on the pipes is selected at 15.6 m/s with a lumped mass of 275, 500, 700, and 1000 kg. The impact velocity value was assumed for sample crash analysis calculations. Mass was assumed to be less than 50% of a compact car. It was supposed that each energy absorber is absorbed kinetic energy equivalent to 275, 500, 700, and 1000 kg mass.

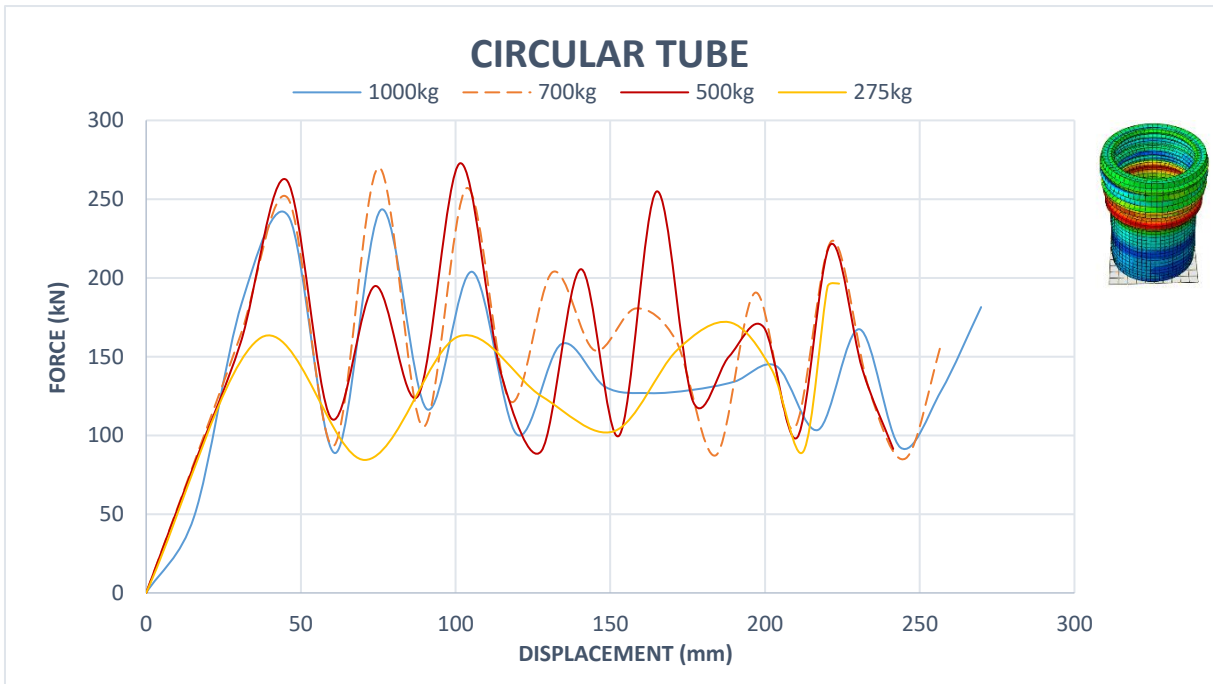
**5. Results**

**5.1. Force-strain diagrams of thin wall structures**

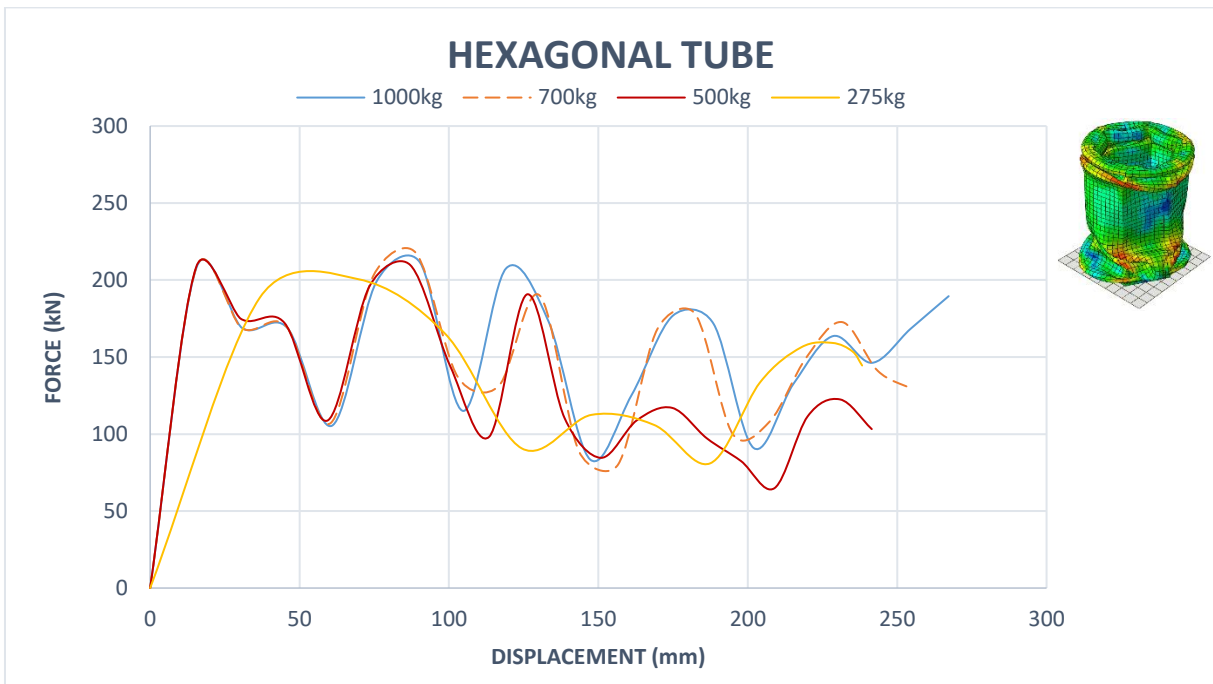
The force-strain values for each type of thin-wall profile were analyzed in this study (Figures 3-6). The displacement values in this study represent the strain of the rigid striker. It is supposed to have full contact with the pipe while the pipe is being crushed. The figures show the force responsible for different profiles owing to the direct loading for the four different forces. It is noticeable from the force-displacement diagrams that the energy is absorbed by the thin-wall structures at the high masses predicted. It is higher than the low mass loadings. Although the graphical oscillations for the four different masses are similar, the energy absorption is higher because the values of the peak forces and average force are higher at higher masses.



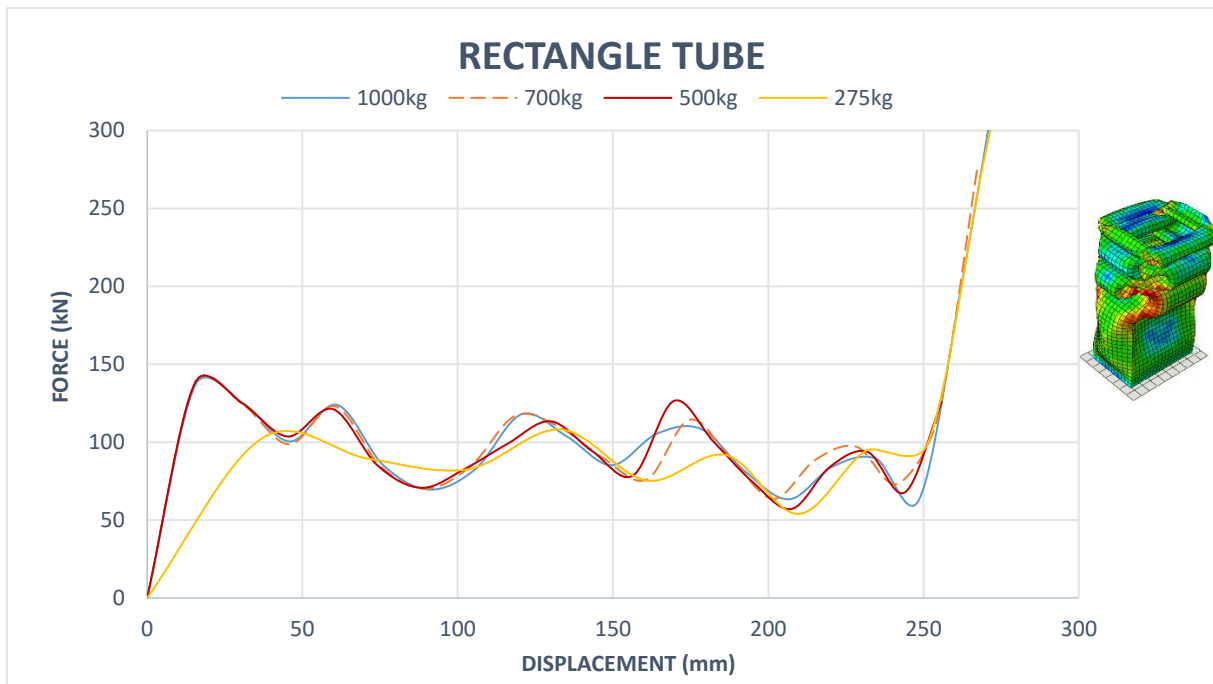
**Figure 3.** Force-displacement for square tube



**Figure 4.** Force-displacement for circular tube



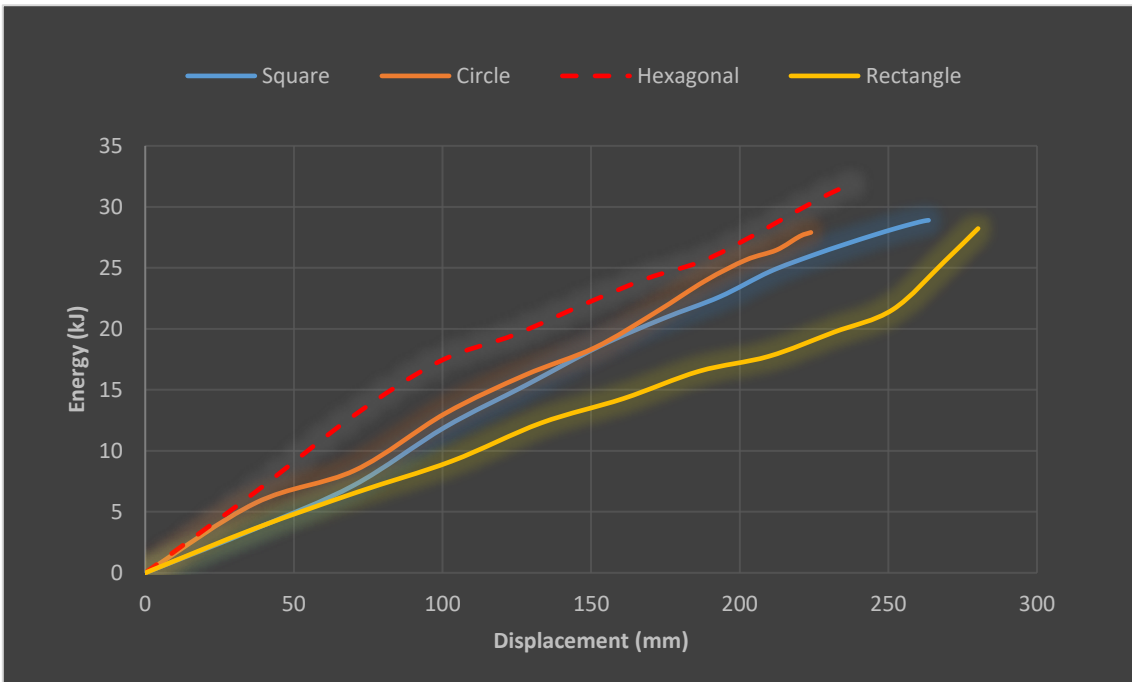
**Figure 5.** Force-displacement for hexagonal tube



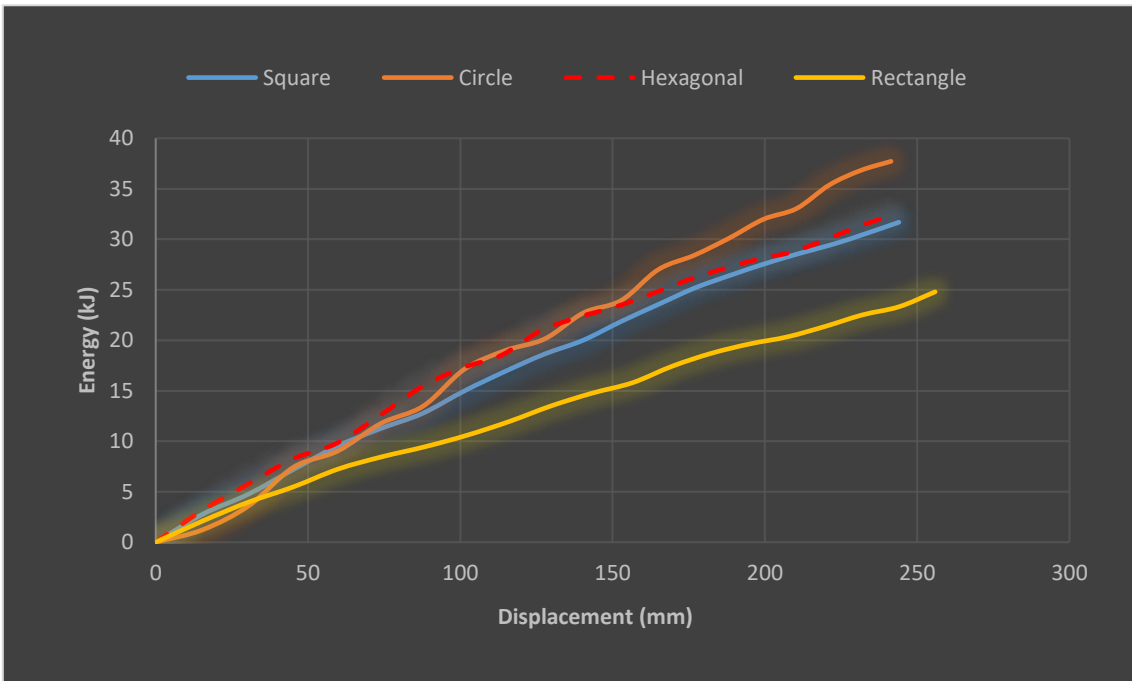
**Figure 6.** Force-displacement for rectangle tube

## 5.2. Energy Absorption

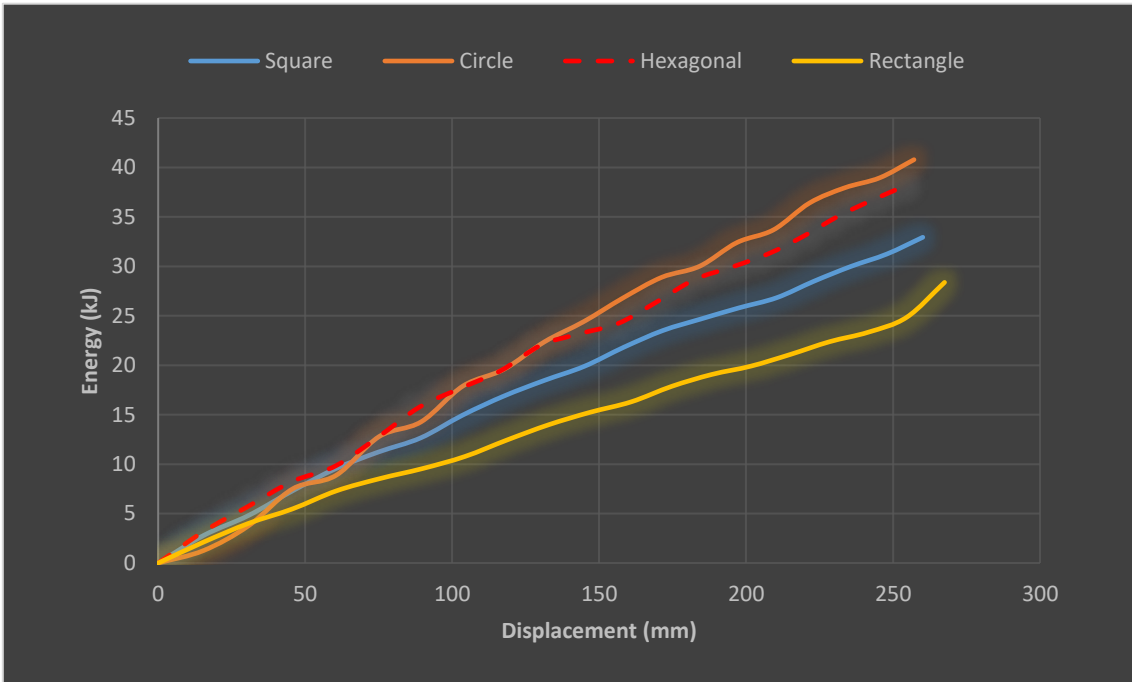
In Figures 7-10, amount of energy absorption is designed as a function of deformation length. It is concluded that the rectangular profile has a highly lower energy absorption capacity than the other three profiles by the energy absorption amounts. Figures 7-10 also show that circular and hexagonal profiles have higher energy absorption capacity. It can be seen from Figure 11 and 12 that the profiles exhibit an overall higher energy absorption capacity when the mass is increased from 275 kg to 1000 kg. However, the circular profile has the highest capacity for 500 kg and 700 kg mass plates.



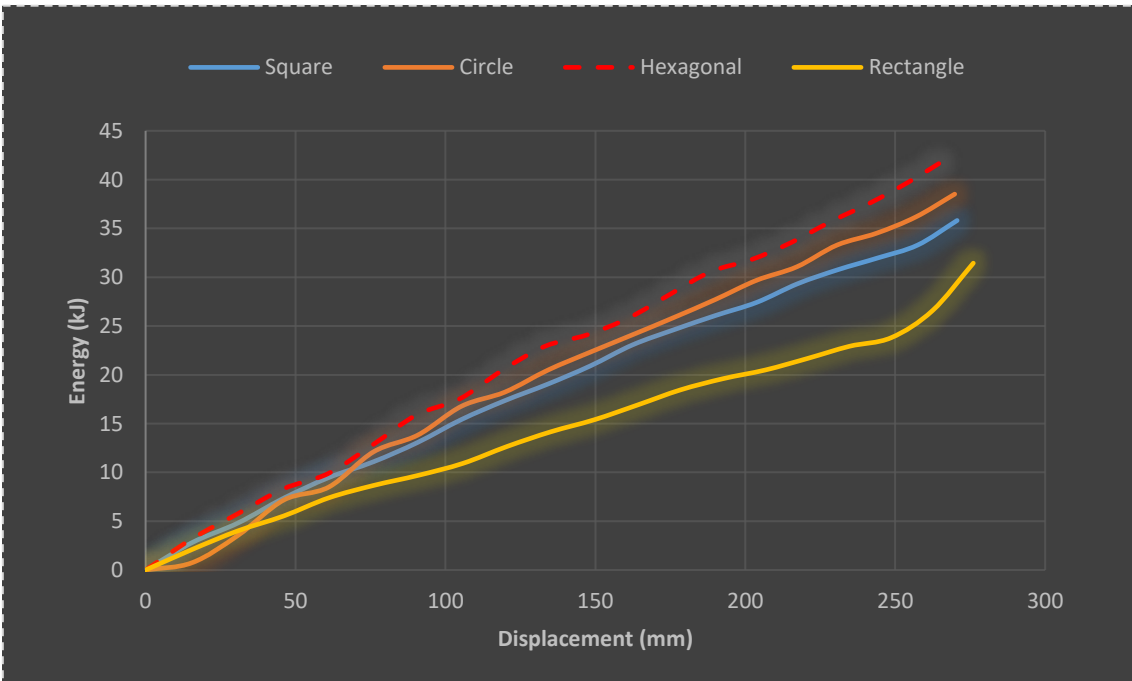
**Figure 7.** Energy absorption capacities of thin wall structures for oblique impact load of 275 kg



**Figure 8.** Energy absorption capacities of thin wall structures for oblique impact load of 500 kg

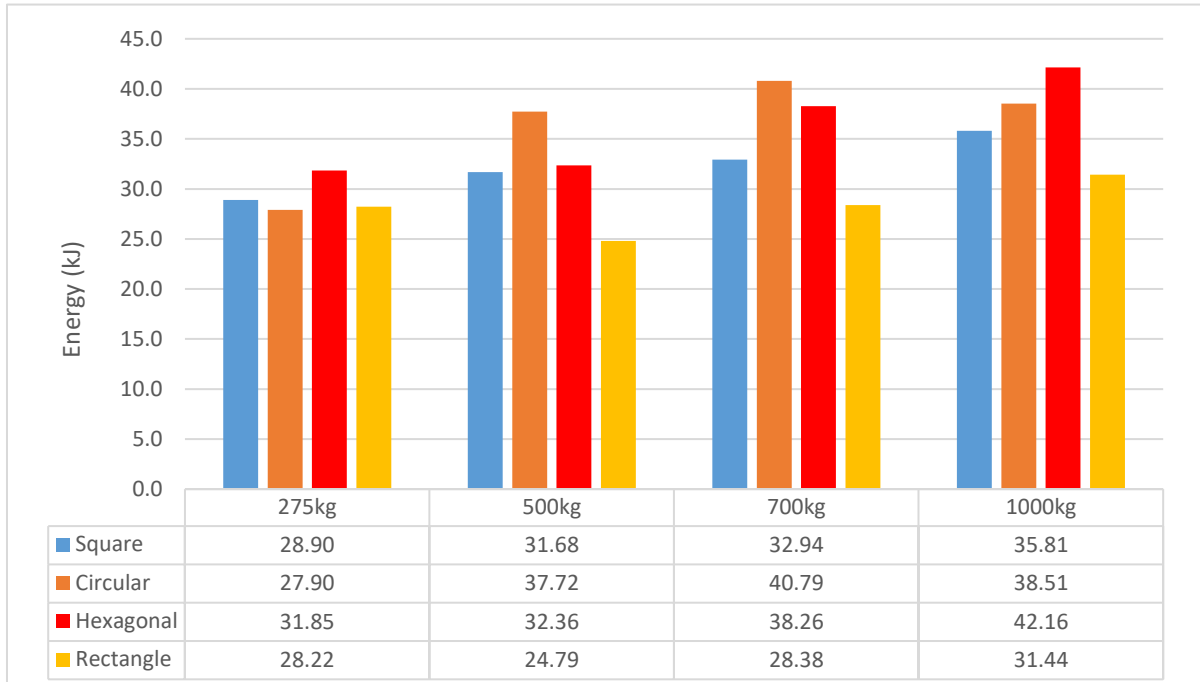


**Figure 9.** Energy absorption capacities of thin wall structures for oblique impact load of 700 kg



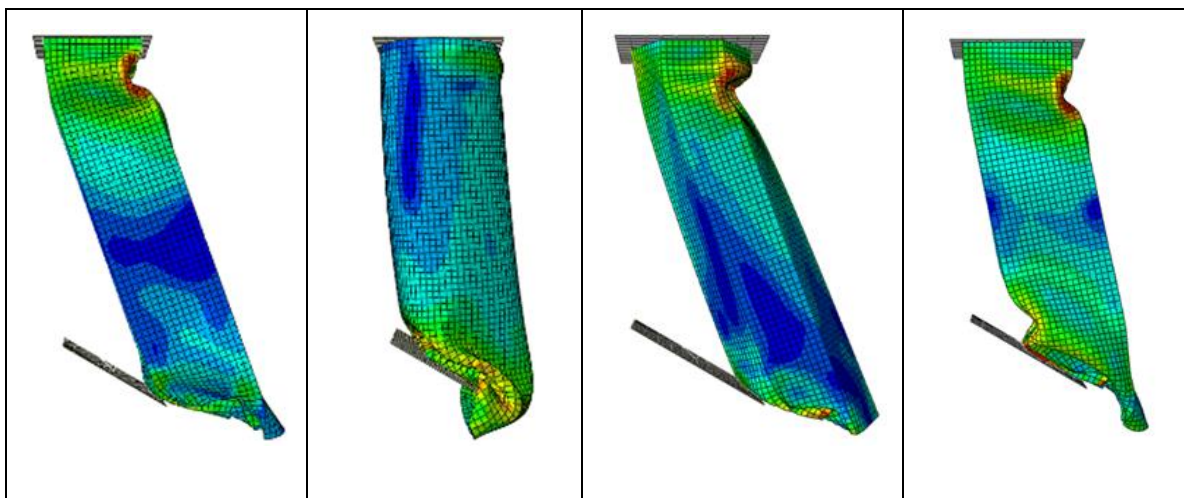
**Figure 2.** Energy absorption capacities of thin wall structures for oblique impact load of 1000 kg





**Figure 3.** Energy absorption capacities for all structures due to direct loading

The lateral loads create more stress points at the corner points of the polygon profiles than the circular cross-section profile. Therefore, these tubes bend more easily than the circular profile and absorb less energy. Circular geometry is the best profile to be considered because it has magnificent capacity in terms of energy absorption in both loading conditions. The finite element analysis results for oblique impact are shown in Figure 12.



**Figure 4.** Finite element analysis results for oblique impact

### 5.3. Velocity–displacement diagrams of different thin wall profiles

In this study, velocity-displacement plots are presented for four profiles (Figure 13). Each profile collided with 275 kg of mass and was analyzed in a 50ms time frame. The reason "why the low mass was chosen to observe the change in velocity that four profiles can stop this mass?" In high mass collisions, the speed is not zero because the tubes cannot absorb the energy completely, and the moving plate is pushed back by the fixed rigid plate due to the action-reaction principle. In these graphs, the circular cross-section profile showed the best result because when the velocity is zero, the profile that deforms least is the circular cross-section profile.

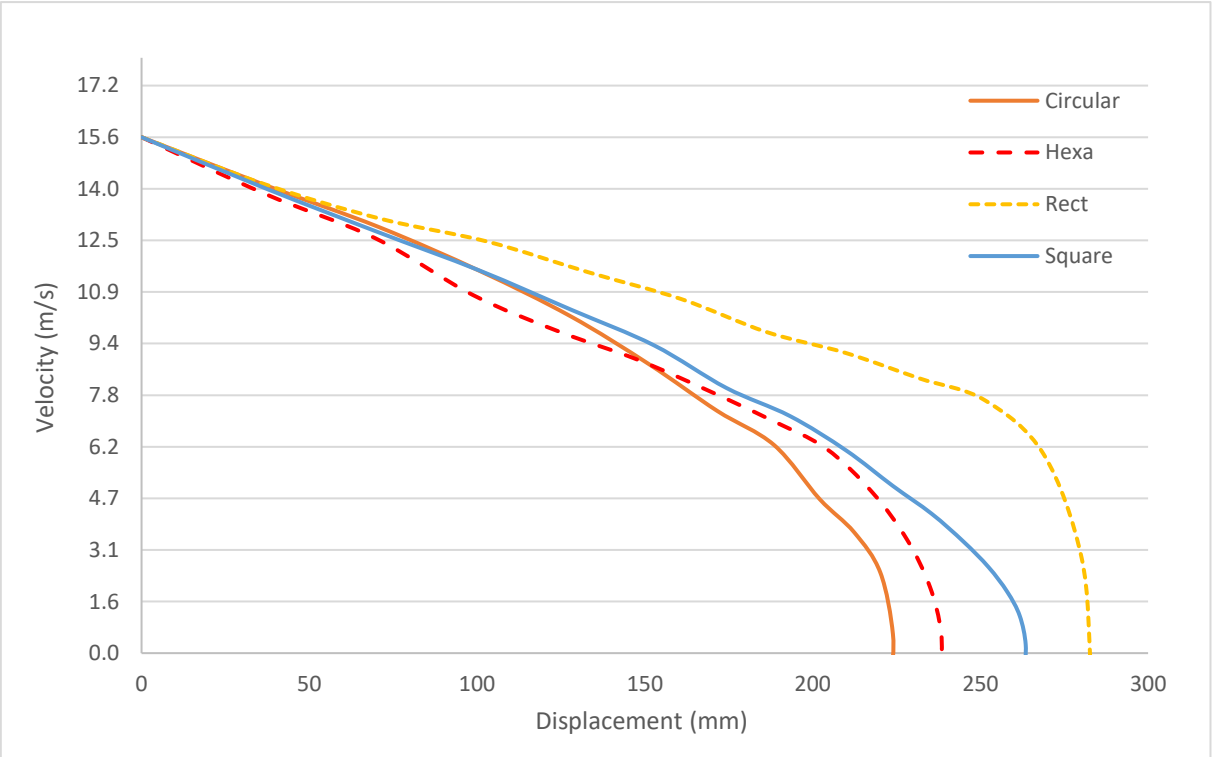


Figure 53. Change in speed of four different profiles for direct impact load of 275 kg

### 6. Findings

In this study, crash analyzes were made on shock absorber models of the safety elements in vehicles. It was determined which profile shock absorber gives better results by considering energy absorption, peak force, CFE, and damping criteria. We numerically investigated axial

and oblique crush responses for four different cross-section profiles of metal alloys (Mild Steel A36). All simulations were dynamic at 15.6 m/s and, oblique loading was investigated at a 30-degree angle.

The reaction forces and energy absorbed increase with the increase of the sheet thicknesses of the bumper elements. Recent studies show that the most suitable sheet thicknesses for bumper elements are 1-3 mm. For this reason, sheet thicknesses were chosen as 2mm. Findings are provided in Table 4.

**Table 4.** Summary of crashworthiness parameters for thin wall tube profiles

Alternatives		Energy (kJ)	F <sub>average</sub> (kN)	F <sub>max</sub> (kN)	CFE
Square	275kg	28.9	81.98	163.94	0.5
	500kg	31.68	122.5	181.95	0.67
	700kg	32.94	124.57	214.14	0.58
	1tone	35.81	135.93	338.37	0.4
Circular	275kg	27.9	77.14	196.32	0.39
	500kg	37.72	152.12	272.79	0.56
	700kg	40.79	148.68	270.09	0.55
	1tone	38.51	139.86	243.41	0.57
Hexagonal	275kg	31.85	86.57	200.61	0.43
	500kg	32.36	127.09	209.74	0.61
	700kg	38.26	146.26	222.96	0.66
	1tone	42.16	157.5	301.41	0.52
Rectangle	275kg	28.2	85.52	380.8	0.22
	500kg	24.79	100.7	273.45	0.37
	700kg	28.38	116.06	401.13	0.29
	1tone	31.44	128.66	511.19	0.25

We observed that the circular profile has a better profile since it absorbs more energy in axial force and absorb more energy by not breaking from stress points in lateral loading. Additionally, when the CFE values of the circular section profile were examined, we can observe that it has similarities to other profiles. Also, the peak force can be reduced by optimizing the tube profile. Thus, the CFE ratio can be increased. But, when we examine the kinetic energy absorption and the CFE values of the rectangular profiles, it is concluded that it is the worst profile.

### 6.1. The MOORA model's result

The MOORA model's result is provided in Table 5. In Table 5, we assigned equal weights for the criteria. In this case, the hexagonal 1-tone alternative has the first rank. We calculated different ranking results using different weight scenarios (Table 6).

**Table 5.** The MOORA model's result

Weight	5	5	5	5	Normalized weights				Yi	Rank
Criteria	Energy (kJ)	F <sub>averag</sub> (kN)	Fmax (KN)	CFE	0.25	0.25	0.25	0.25		
Alternatives										
s275kg	28.9	81.98	163.94	0.5	0.054	0.042	0.036	0.063	0.194	15
s500kg	31.68	122.5	181.95	0.67	0.059	0.062	0.039	0.085	0.245	9
s700kg	32.94	124.57	214.14	0.58	0.061	0.063	0.046	0.074	0.244	10
s1tone	35.81	135.93	338.37	0.4	0.067	0.069	0.073	0.051	0.259	7
c275kg	27.9	77.14	196.32	0.39	0.052	0.039	0.043	0.049	0.183	16
c500kg	37.72	152.12	272.79	0.56	0.07	0.077	0.059	0.071	0.277	3
c700kg	40.79	148.68	270.09	0.55	0.076	0.075	0.058	0.07	0.279	2
c1tone	38.51	139.86	243.41	0.57	0.072	0.071	0.053	0.072	0.267	5
h275kg	31.85	86.57	200.61	0.43	0.059	0.044	0.043	0.055	0.201	14
h500kg	32.36	127.09	209.74	0.61	0.06	0.064	0.045	0.077	0.247	8
h700kg	38.26	146.26	222.96	0.66	0.071	0.074	0.048	0.084	0.277	4
h1tone	42.16	157.5	301.41	0.52	0.078	0.08	0.065	0.066	0.289	1
r275kg	28.2	85.52	380.8	0.22	0.052	0.043	0.082	0.028	0.206	12
r500kg	24.79	100.7	273.45	0.37	0.046	0.051	0.059	0.047	0.203	13
r700kg	28.38	116.06	401.13	0.29	0.053	0.059	0.087	0.037	0.235	11
r1tone	31.44	128.66	511.19	0.25	0.058	0.065	0.111	0.032	0.266	6
$\sqrt{\sum_{j=1}^m x_{ij}^2}$	134.39	493.76	1154.25	1.97						

**Very important: 10**  
**Important: 8**  
**Medium Important: 5**  
**Low important: 3**  
**Very low important:1**

**Table 6.** Scenario analysis

Alternatives	Scenarios					Ranking differences									
	A	B	C	D	E	A-B	A-C	A-D	A-E	B-C	B-D	B-E	C-D	C-E	D-E
s275kg	15	14	15	16	9	1	0	-1	6	-1	-2	5	-1	6	7
s500kg	9	10	10	13	2	-1	-1	-4	7	0	-3	8	-3	8	11
s700kg	10	7	9	11	7	3	1	-1	3	-2	-4	0	-2	2	4
s1tone	7	6	6	4	10	1	1	3	-3	0	2	-4	2	-4	-6
c275kg	16	15	16	15	12	1	0	1	4	-1	0	3	1	4	3
c500kg	3	5	2	6	5	-2	1	-3	-2	3	-1	0	-4	-3	1
c700kg	2	2	3	7	6	0	-1	-5	-4	-1	-5	-4	-4	-3	1
c1tone	5	4	5	8	4	1	0	-3	1	-1	-4	0	-3	1	4
h275kg	14	11	14	14	11	3	0	0	3	-3	-3	0	0	3	3
h500kg	8	9	8	12	3	-1	0	-4	5	1	-3	6	-4	5	9
h700kg	4	3	4	10	1	1	0	-6	3	-1	-7	2	-6	3	9
h1tone	1	1	1	5	8	0	0	-4	-7	0	-4	-7	-4	-7	-3
r275kg	12	13	13	3	16	-1	-1	9	-4	0	10	-3	10	-3	-13
r500kg	13	16	12	9	13	-3	1	4	0	4	7	3	3	-1	-4
r700kg	11	12	11	2	14	-1	0	9	-3	1	10	-2	9	-3	-12
r1tone	6	8	7	1	15	-2	-1	5	-9	1	7	-7	6	-8	-14
					r <sub>s</sub>	0.935	0.988	0.497	0.503	0.932	0.329	0.574	0.479	0.515	-0.403
					Z	<b>3.622</b>	<b>3.827</b>	<b>1.925</b>	<b>1.948</b>	<b>3.611</b>	<b>1.276</b>	<b>2.221</b>	<b>1.857</b>	<b>1.993</b>	<b>-1.561</b>

- A: All criteria are equally weighted
- B: Energy criterion is the most important others are very low important
- C: F<sub>average</sub> criterion is the most important others are very low important
- D: F<sub>max</sub> criterion is the most important others are very low important
- E: CFE criterion is the most important others are very low important

In this section, the ranking results obtained by the MOORA method are compared with the results obtained by the different scenarios (Table 6). Results were analyzed using Spearman's rank correlation test [35]. Spearman's rank correlation test can be applied using the following equations:

$$d^k = x^k - y^k, \quad k=1, \dots, K \quad (11)$$

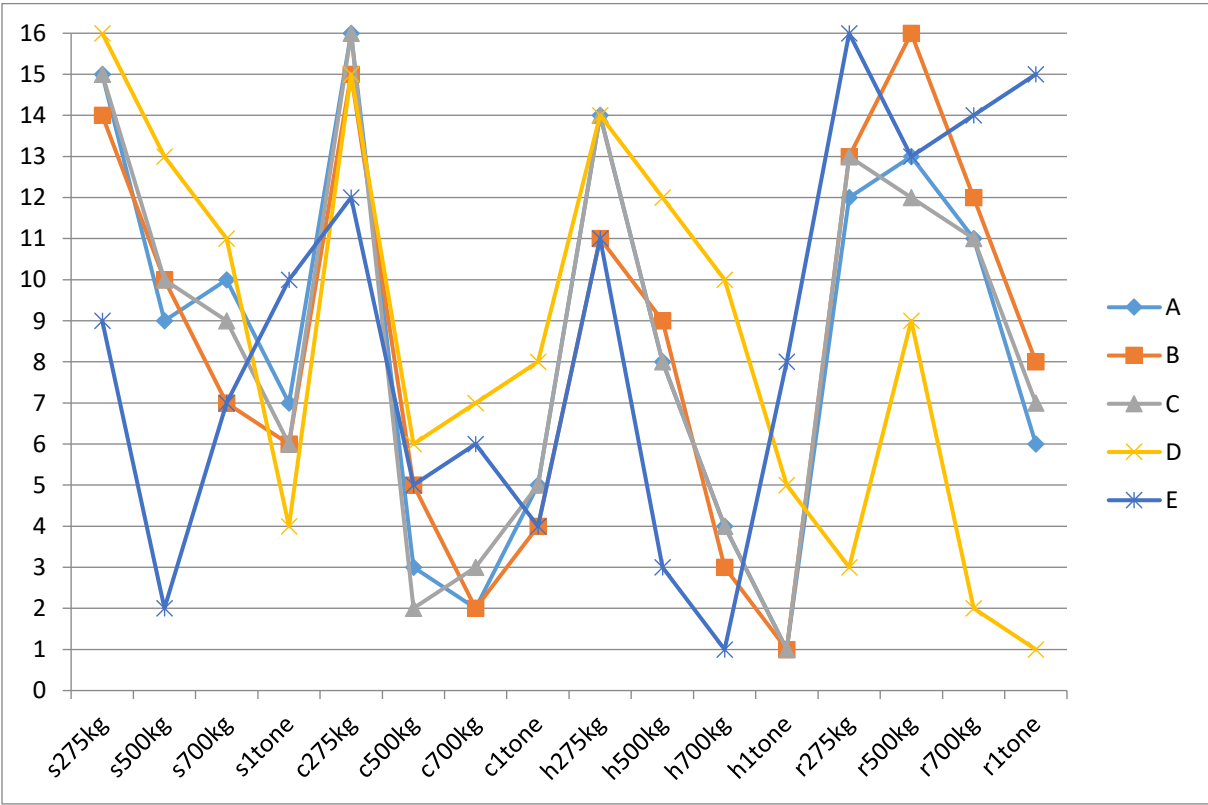
$$r_s = 1 - \left\{ 6 \cdot \left[ \sum_{k=1}^K \frac{(d^k)^2}{K \cdot (K^2 - 1)} \right] \right\} \quad (12)$$

$$Z = r_s \cdot \sqrt{(K - 1)} \quad (13)$$

In equations; d<sup>k</sup>: The difference between the two data set values; K : Number of data; Z : It is defined as a test statistic.

For consistency between the two rankings, the Z value is expected to be above 1.645 at the 95% confidence level ( $\alpha=0.05$ ). The Z values of the MOORA ranking results were calculated above 1.645, except for B-D and D-E comparisons. So, the ranking results are dissimilar for scenario D. Scenario E also has different ranking results. But, it provides a statistically similar ranking when compared to other scenarios.

On the other hand, the first three rankings are differentiated using the different weight values (Figure 5). Circular profiles (for 500kg, 700 kg, 1- tone cases), hexagonal profiles (for 500kg, 700kg, 1- tone cases), and rectangle profiles (r275kg, r500kg, r700kg, r 1 tone cases) has the first three rankings for different scenarios (Figure 14).



**Figure 14.** Ranking result comparison for scenario analysis

## 7. Conclusion

In conclusion, it can be said that the circular tube profile has a high potential as a good energy absorber candidate in terms of helping to reduce serious injuries to the vehicle occupant and in terms of crash resistance. Although each profile shows the same velocity-displacement behavior, the circular profile has a lower deformation rate compared to the other profiles.

Hexagonal and circular profiles have the best performances for energy,  $F_{\text{average}}$ , and CFE criteria as a result of the MOORA model. On the other hand, a rectangular profile is the best one considering the  $F_{\text{max}}$  criteria. In Table 7, we figured most suitable alternatives for different cases.

Different material types (metal or composite) and their specifications can be investigated in future studies. Also, different MCDM models can be incorporated into the study for the ranking process depending on the criteria types, criteria number, and alternative structure types.

**Table 7.** Final analysis for results

	Scenarios				
	A	B	C	D	E
Alternatives	Equal Importance	Energy (kJ)	$F_{\text{average}}$ (kN)	$F_{\text{max}}$ (kN)	CFE
s500kg					2
c500kg	3		2		
c700kg	2	2	3		
h500kg					3
h700kg		3			1
h1tone	1	1	1		
r275kg				3	
r700kg				2	
r1tone				1	

## Declarations

## Conflict of interest

The authors declare no competing interests.

## References

1. Kumar, K. and M. Puneeth, *Study of Two-distinct Automotive Bumper Beam Designs during Low speed impacts*.
2. Kurtuluş, E. and G. Tekin, *Conversion of Aluminum Front Bumper System to Magnesium Material by Using Design of Experiment Method*. International Journal of Automotive Science And Technology, 2021. **5**(1): p. 34-42.
3. Zhang, Y., J. Wang, and C. Ma, *Research on Reconstruction of Frontal Collision Accidents of Two Cars Based on the Combination of PC-crash and Finite Element Method*. Converter, 2021. **2021**(7): p. 721-732.
4. Li, Q., et al., *Improve the frontal crashworthiness of vehicle through the design of front rail*. Thin-Walled Structures, 2021. **162**: p. 107588.
5. Luo, C., et al., *Design, manufacturing and applications of auxetic tubular structures: A review*. Thin-Walled Structures, 2021. **163**: p. 107682.
6. Kale, T. and G. Gulwade, *Study and Design of Front Bumper for Light Motor and Heavy Motor Vehicles*. 2021.
7. Sinha, S., S. Tewari, and R. Dhawan, *Crash Analysis of the Frontal Structure of a Car Using Explicit Dynamics*. Turkish Journal of Computer and Mathematics Education (TURCOMAT), 2021. **12**(14): p. 1627-1634.
8. Basith, M.A., et al., *Crash analysis of a passenger car bumper assembly to improve design for impact test*. Materials Today: Proceedings, 2021. **45**: p. 1684-1690.
9. Khedkar, N.K., C. Sonawane, and S. Kumar, *Experimental and static numerical analysis on bumper beam to be proposed for Indian passenger car*. Materials Today: Proceedings, 2021. **42**: p. 383-387.
10. Aşkar, M.T. and K. Ermiş, *Crash Analysis and Size Optimization of a Vehicle's Front Bumper System*. International Journal of Automotive Science And Technology. **5**(3): p. 184-191.
11. Lei, F., et al., *Nondeterministic multi-objective and multi-case discrete optimization of functionally-graded front-bumper structures for pedestrian protection*. Thin-Walled Structures, 2021. **167**: p. 106921.
12. Sun, G., et al., *Parallelized optimization design of bumper systems under multiple low-speed impact loads*. Thin-Walled Structures, 2021. **167**: p. 108197.



13. Wang, H., et al., *Implementation of a novel Six Sigma multi-objective robustness optimization method based on the improved response surface model for bumper system design*. Thin-Walled Structures, 2021. **167**: p. 108257.
14. Kim, Y., et al., *Behavior of dragon skin flexible metal bumper under hypervelocity impact*. International Journal of Impact Engineering, 2019. **125**: p. 13-26.
15. Wang, C., et al., *Structure design and multi-objective optimization of a novel crash box based on biomimetic structure*. International Journal of Mechanical Sciences, 2018. **138**: p. 489-501.
16. Huang, X., et al., *Hypervelocity impact of TiB<sub>2</sub>-based composites as front bumpers for space shield applications*. Materials & Design, 2016. **97**: p. 473-482.
17. Higashide, M., et al., *Comparison of aluminum alloy and CFRP bumpers for space debris protection*. Procedia Engineering, 2015. **103**: p. 189-196.
18. Liu, Z., J. Lu, and P. Zhu, *Lightweight design of automotive composite bumper system using modified particle swarm optimizer*. Composite Structures, 2016. **140**: p. 630-643.
19. Ren, S., et al., *A reactive material double-bumper shield for centimeter sized projectile*. International Journal of Impact Engineering, 2021. **158**: p. 104028.
20. Selwyn, T.S., *Formation, characterization and suitability analysis of polymer matrix composite materials for automotive bumper*. Materials Today: Proceedings, 2021. **43**: p. 1197-1203.
21. Muthalagu, R., et al., *Tensile attributes and material analysis of kevlar and date palm fibers reinforced epoxy composites for automotive bumper applications*. Materials Today: Proceedings, 2021. **46**: p. 433-438.
22. Godara, S. and S.N. Nagar, *Analysis of frontal bumper beam of automobile vehicle by using carbon fiber composite material*. Materials Today: Proceedings, 2020. **26**: p. 2601-2607.
23. Goyal, S., et al., *Crashworthiness analysis of foam filled star shape polygon of thinwalled structure*. Thin-Walled Structures, 2019. **144**: p. 106312.
24. G Keni, L., et al., *Conceptual design and analysis of a car bumper using finite element method*. Cogent Engineering, 2021. **8**(1): p. 1976480.

25. Zhang, X., *Crashworthiness Characterisation of the Car Front Bumper System Based on FEA Analysis*. 2020.
26. Wang, Y., *Performance Analysis of Front Bumper under Frontal Low Speed Impact*. Open Access Library Journal, 2021. **8**(1): p. 1-12.
27. Natarajan, N., P. Joshi, and R. Tyagi, *Design improvements of vehicle bumper for low speed impact*. Materials Today: Proceedings, 2021. **38**: p. 456-465.
28. Reiner, J., N. Zobeiry, and R. Vaziri, *Efficient finite element simulation of compression after impact behaviour in quasi-isotropic composite laminates*. Composites Communications, 2021: p. 100967.
29. Ataabadi, P., D. Karagiozova, and M. Alves, *Finite element modeling of crushing of CFRP cylindrical tubes under low-velocity axial impact*. Composite Structures, 2021: p. 114902.
30. Graba, M., et al., *Impact of the acceleration intensity of a passenger car in a road test on energy consumption*. Energy, 2021. **226**: p. 120429.
31. Chakraborty, S. *Applications Of The MOORA Method For Decision Making In Manufacturing Environment*. The International Journal of Advanced Manufacturing Technology, 2011. P.1155-1166.
32. Brauers, M., Ginevicius, R., Podvezko, V. *Regional development in Lithuania considering multiple objectives by the MOORA method*, Technol Econ Dev Econ, 2010. P. 613–640.
33. Brauers, M., Zavadskas, E. *The MOORA Method And Its Application To Privatization In A Transition Economy*, Control and Cybernetics, 2006. **35**(2): p. 1-5.
34. Tarlochan, F., et al., *Design of thin wall structures for energy absorption applications: Enhancement of crashworthiness due to axial and oblique impact forces*. Thin-Walled Structures, 2013. **71**: p. 7-17.
35. Ic, Y.T., Yurdakul, M. *Analysis of the effect of the number of criteria and alternatives on the ranking results in applications of the multi criteria decision making approaches in machining center selection problems*. Journal of the Faculty of Engineering and Architecture of Gazi University, 2020. **35**(2) p. 991-1001.